

# Spin transport in an electrically-driven magnon gas near Bose-Einstein condensation: a Hartree-Fock-Keldysh theory

So Takei\*

*Department of Physics, Queens College of the City University of New York, Queens, NY 11367, USA and  
Physics Doctoral Program, Graduate Center of the City University of New York, New York, NY 10016, USA*

(Dated: September 8, 2022)

An easy-plane ferromagnetic insulator in a uniform external magnetic field and in contact with a phonon bath and a normal metal bath is studied theoretically in the presence of dc spin current injection via spin Hall effect in the metal. The Keldysh path integral formalism is used to model the magnon gas driven into nonequilibrium steady state by mismatched bath temperatures and/or electrical spin injection, and we analyze the magnon system in the normal (uncondensed) state, but close to field- and electrically-driven instability to Bose-Einstein condensation (BEC), within the self-consistent Hartree-Fock approximation. We show that the BEC instability in the electrically-driven magnon system is signaled by a sign change in the imaginary part of the poles for long-wavelength magnon modes and by the divergence of the nonequilibrium magnon distribution function. In the presence of two bath temperatures, we find that the correlation length of the superfluid order parameter fluctuations exhibits nontrivial finite temperature crossover behavior that is richer than the standard crossover behavior obtained for the vacuum-superfluid transition in an equilibrium dilute Bose gas. We study the consequences of these thermal crossovers on the magnon spin conductivity and obtain an inverse square-root divergence in the spin conductivity in the vicinity of the electrically-induced BEC instability. A spintronics device capable of testing our spin transport predictions is discussed.

## I. INTRODUCTION

Magnetically-ordered insulators provide an attractive arena to study nonequilibrium Bose-Einstein condensation (BEC) of magnons in a dissipative solid state environment.<sup>1,2</sup> Unlike BECs in ultra-cold atomic systems and superconductors, quasiparticle BECs in solids typically require nonequilibrium states in which the systems are externally pumped with sufficient energy to compensate for the incessant quasiparticle decay.<sup>3,4</sup> An early spectroscopic evidence for room temperature magnon BEC was reported in a ferrimagnetic insulator yttrium iron garnet (YIG) driven by parametric pumping.<sup>5-7</sup> According to the prevailing heuristic picture, the magnon BEC forms during a *transient* stage after a sufficient number of hot incoherent magnons are injected into a narrow region of the spectrum and the pump is switched off.<sup>8,9</sup> Magnons rapidly thermalize to a quasi-equilibrium state via multi-magnon scattering processes and condense before they ultimately decay into the lattice.

An alternative pumping mechanism is dc electrical pumping, which involves interfacing the magnetic insulator to a normal metal with strong spin-orbit coupling and utilizing spin Hall effect in the metal for spin injection.<sup>10,11</sup> In the presence of exchange coupling between the two subsystems, magnon injection (absorption) occurs via the annihilation (creation) of spinful particle-hole excitations in the metal so that the metal serves both as a spin injector and a dissipative environment. Here, the threshold injection strength necessary for magnon condensation can be attained by increasing the electrical current inside the normal metal. An interesting aspect of this proposal is the possibility to realize a magnon BEC in a nonequilibrium *steady state*, a flow-equilibrium state in which spin lost into the dissipative environment is precisely compensated by spin injection from the metal.<sup>10,11</sup>

Motivated by this proposal, a recent experiment achieved BEC criticality via electrical spin injection in a bilayer sys-

tem consisting of YIG and heavy-element metal platinum (Pt). The experiment reported a significant increase in the two-terminal dc magnon spin conductivity above the critical magnon density and a compelling evidence for dissipationless spin transport mediated by a magnon condensate.<sup>12</sup> This exciting development calls for a detailed study of spin transport through magnon gases in the vicinity of the BEC transition and in the simultaneous presence of dissipation and electrical pumping.

On a broader note, quasiparticle BECs in driven-dissipative steady states have been studied extensively in the context of photons<sup>13</sup>, excitons in coupled quantum Hall bilayers<sup>14</sup> and exciton-polaritons in light-driven semiconductor heterostructures<sup>15</sup>. In the context of exciton-polariton systems, the Keldysh path integral formalism has proved useful for systematically analyzing the effects of the external pump and dissipation in the self-consistent mean-field description of the coherent state and of the fluctuations beyond the mean-field limit.<sup>16</sup> This powerful theoretical machinery is beginning to be applied to the nonequilibrium magnon BEC phenomenon<sup>17</sup> and could be useful in rigorously addressing the properties of a magnon gas tuned close to the BEC transition in a driven-dissipative environment. This approach should not only elucidate the combined effects of dissipation and nonequilibrium drive on the BEC instability criteria but also on the finite temperature crossover behaviors and spin transport properties of near-critical magnon gases. Furthermore, the BEC transition of ferromagnetic exchange magnons belongs to the same universality class as the vacuum-superfluid phase transition in dilute Bose gases in thermal equilibrium.<sup>18</sup> The rigorous theoretical formulation of nonequilibrium magnon BEC should then set the stage for studying how departures from thermal equilibrium and particle/energy conservation modify the behavior of Bose gases near this well-known phase transition.

In this work, we formulate a Keldysh path integral the-

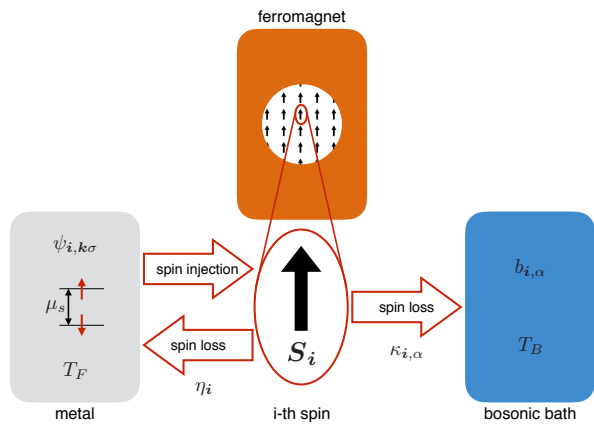


FIG. 1. (Color online) Each atomic spin at site  $i$  of the ferromagnetic insulator is coupled to its own phonon and metallic baths with coupling strengths  $\eta_i$  and  $\kappa_{i,\alpha}$ , respectively. The phonon bath is characterized by excitations  $b_{i,\alpha}$ , where  $\alpha$  labels the eigenmodes, and the metallic bath is characterized by fermion excitations  $\psi_{i,k\sigma}$  with wavevector  $k$  and spin  $\sigma$ . We assume the two baths are thermalized at different temperatures  $T_F$  and  $T_B$ , and a nonequilibrium spin accumulation  $\mu_s$  in the metal allows for spin injection into the ferromagnet.

ory for a driven-dissipative easy-plane ferromagnetic insulator coupled to a bosonic (phonon) bath and a metallic bath, both of which introduces spin/energy loss (i.e., Gilbert damping) within the ferromagnet. A nonequilibrium spin accumulation in the metal (generated, e.g., via spin Hall effect) also allows for incoherent spin injection (dc electrical pumping) into the magnet. Starting from a microscopic Keldysh action consisting of the magnetic subsystem and the baths, the reduced Keldysh action for the active magnons alone is obtained by tracing out the bath degrees of freedom. Based on the resulting effective magnon action, we focus exclusively on the normal (uncondensed) phase near the BEC criticality for various bath temperatures and electrical pumping strengths, and account for the quartic magnon-magnon interaction term within the self-consistent Hartree-Fock approximation.

We find that the steady state magnon distribution function, for mismatched bath temperatures and/or electrical pumping, generally has a non-thermal form that cannot be described by a single effective chemical potential and effective temperature but is given by a nontrivial weighted superposition of the bath distribution functions. We also quantify the shift in the position of the BEC critical line as a function of bath temperatures and electrical pumping, and find that the correlation length of the superfluid critical fluctuations possesses crossover behaviors with respect to finite bath temperatures that are richer than those predicted for equilibrium dilute Bose gases near BEC criticality.<sup>18</sup>

In the latter part of the work, we shift our focus to spin transport and compute the magnon spin conductivity for the magnon gas using the Kubo formalism and within the Hartree-Fock approximation. We first investigate how the above-mentioned finite temperature crossover behaviors in the correlation length are reflected in spin transport. Specifically, for

zero electrical pumping, we find that the spin conductivity traverses through three different thermal regimes, each with a distinct temperature dependence, as the bath temperatures are increased from absolute zero. For finite pumping, we find an inverse square-root divergence of the spin conductivity as the dc electrical pumping strength approaches the threshold value for BEC instability. Motivated by the recent spin transport experiment on magnon gases close to the electrically-driven BEC instability,<sup>12</sup> we discuss how our spin transport predictions can be verified using a similar experimental setup.

The paper is organized as follows. In Sec. II, we introduce the models for the magnetic system of interest and the baths, and obtain an effective theory for the magnons alone by tracing out all of the bath degrees of freedom using the Keldysh functional integral formalism. In Sec. III, we develop a self-consistent Hartree-Fock theory for the magnon system, and study the BEC critical line and the finite temperature crossover behavior. Spin conductivity is computed in Sec. IV, and a discussion on how the conductivity can be verified in a two-terminal spin transport setup is presented in Sec. V. Conclusions are drawn in Sec. VI.

## II. MODEL AND THEORY

The system of interest consists of a 3-dimensional ferromagnetic insulator coupled to both bosonic and metallic (fermionic) baths (see Fig. 1). The former is introduced to explicitly model the intrinsic spin/energy loss (i.e., Gilbert damping) within the ferromagnet, while the latter leads to additional Gilbert damping due to the fermionic continuum. A nonequilibrium spin accumulation  $\mu_s$  in the metal (generated, e.g., via the spin Hall effect) also allows for incoherent spin injection into the magnetic insulator. Since we focus on the impact of dissipation and nonequilibrium drive on the magnetic subsystem, we consider a relatively simple, but quite general, model Hamiltonian for an exchange ferromagnet with an easy-plane magnetic anisotropy perpendicular to the  $z$  axis and in a uniform magnetic field  $B$  along the same axis. The Hamiltonian for the full system can then be written as  $H = H_F + \sum_i \mathcal{H}_i$ , where

$$H_F = \frac{1}{2} \sum_{ij} [-J_{ij} \mathbf{S}_i \cdot \mathbf{S}_j + K_{ij} S_i^z S_j^z] + \hbar\gamma B \sum_i S_i^z \quad (1)$$

models the ferromagnet, and  $\mathcal{H}_i$  (defined later) is a local Hamiltonian describing the coupling of the atomic spin at site  $i$  to the baths. Here,  $i, j$  label the sites of the lattice,  $J_{ij} > 0$  is the ferromagnetic exchange matrix,  $K_{ij} > 0$  is the anisotropy matrix,  $\gamma$  is the gyromagnetic ratio and  $S$  is the saturated spin moment per lattice site. We assume throughout that both  $J_{ij}$  and  $K_{ij}$  depend on the lattice positions  $\mathbf{R}_i$  and  $\mathbf{R}_j$  only through their difference, and that  $J_{ij} = J_{ji}$  and  $K_{ij} = K_{ji}$ . Furthermore, for a spherically symmetric exchange constant  $J_{ij} \propto e^{-|\mathbf{R}_i - \mathbf{R}_j|^2 / 2\xi_J^2}$  with a spatial range  $\xi_J$ , we may approximate its Fourier transform as  $J_q = \sum_j J_{ij} e^{-iq \cdot (\mathbf{R}_i - \mathbf{R}_j)} = J_0 e^{-q^2 \xi_J^2 / 2}$ , where  $J_0 \equiv J_{q=0}$ . A similar result can be applied to a spherically symmetric anisotropy constant  $K_{ij}$  with a spatial range

of  $\xi_K$ , i.e.,  $K_q \approx K_0 e^{-q^2 \xi_K^2/2}$ .

Following the standard boson mapping,<sup>19</sup> Eq. (1) can be re-expressed in terms of creation and annihilation operators for magnons with wavevector  $\mathbf{q}$ ,  $a_q^\dagger$  and  $a_q$ , i.e.,

$$H_F = \sum_{\mathbf{q}} (\varepsilon_{\mathbf{q}} + \mu_0) a_{\mathbf{q}}^\dagger a_{\mathbf{q}} + \frac{1}{\mathcal{N}} \sum_{\{q_n\}} V_{q_1 q_3} a_{q_1}^\dagger a_{q_2}^\dagger a_{q_3} a_{q_4} \delta_{q_1+q_2, q_3+q_4}, \quad (2)$$

where  $\varepsilon_{\mathbf{q}} = S(J_0 - J_{\mathbf{q}}) \approx (J_0 S \xi_J^2/2) q^2$ , valid for  $q \ll \xi_J^{-1}$ , is the magnon spectrum,  $\mu_0 = \hbar\gamma B - S K_0$  is the bare magnon gap (tunable using the external field), and  $\mathcal{N}$  is the total number of lattice sites in the ferromagnet. The 4-magnon vertex here takes the form

$$V_{q_1 q_3} = \frac{K_{q_1-q_3} - J_{q_1-q_3}}{2} + \lambda(J_{q_1} + J_{q_3}),$$

where  $\lambda = S(1 - \sqrt{1 - 1/2S})$ .

We now define the spin-bath coupling. As shown in Fig. 1, we assume that the atomic spin on each lattice site  $\mathbf{i}$  couples to its own *independent* bosonic and fermionic baths. The local Hamiltonian may then be written as  $\mathcal{H}_i = \mathcal{H}_i^B + \mathcal{H}_i^m$ , where  $\mathcal{H}_i^B$  and  $\mathcal{H}_i^m$  model the coupling to the bosonic and fermionic baths, respectively. We write the bosonic contribution as

$$\mathcal{H}_i^B = \sum_{\alpha} \hbar\Omega_{\alpha} b_{i,\alpha}^\dagger b_{i,\alpha} + \hbar \sum_{\alpha} [\kappa_{i,\alpha} a_i b_{i,\alpha}^\dagger + h.c.],$$

where  $b_{i,\alpha}$  is the annihilation operator for a boson in eigenmode  $\alpha$  in the  $i$ -th bath, which couples to the magnon at the site with strength  $\kappa_{i,\alpha}$ . The second term describes the decay of a magnon into the bath by transmuted into a superposition of bath boson modes. We assume that all of the bosonic baths are identical and that they are held at the same temperature  $T_B$  so that the excitations occupy the states according to the Bose-Einstein distribution, i.e.,  $\langle b_{i,\alpha}^\dagger b_{i,\alpha'} \rangle = n_{\alpha} \delta_{\alpha\alpha'}$ , where  $n_{\alpha} = (e^{\hbar\Omega_{\alpha}/k_B T_B} - 1)^{-1}$ . We hereafter refer to the bosonic excitations as *phonons* and  $T_B$  as the phonon temperature. In the absence of the metal (and, therefore, driving), the magnons thermalize to the Bose-Einstein distribution of the phonons.

The metallic bath contribution to the local Hamiltonian can be written as

$$\mathcal{H}_i^m = \sum_{k,\sigma} \hbar v_k \psi_{i,k\sigma}^\dagger \psi_{i,k\sigma} + \sum_{k,k'} [\eta_i \psi_{i,k\uparrow}^\dagger \psi_{i,k'\downarrow} a_i + h.c.],$$

where  $\psi_{i,k\sigma}$  annihilates a fermion in the  $i$ -th bath with wavevector  $\mathbf{k}$  and spin  $\sigma$ ,  $\hbar v_k = \hbar^2 k^2/2m$  is the usual quadratic spectrum with effective mass  $m$ , and  $\eta_i$  quantifies the hybridization between the magnon and the fermions at site  $\mathbf{i}$ . We assume that all of the fermionic baths are identical and that they are held a common temperature  $T_F$  so that the excitations occupy the states according to the Fermi-Dirac distribution  $\langle \psi_{i,k\sigma}^\dagger \psi_{i,k'\sigma'} \rangle = f_{k\sigma} \delta_{\sigma\sigma'} \delta_{kk'}$ , where  $f_{k\sigma} = [e^{(\hbar v_k - \mu_{\sigma})/k_B T_F} + 1]^{-1}$ . Here,  $\mu_{\sigma}$  is the spin-dependent chemical potential that models the nonequilibrium spin accumulation  $\mu_s$  inside the metal, i.e.,  $\mu_s = \mu_{\uparrow} - \mu_{\downarrow}$ .

## A. Keldysh path integral formulation

Long after the couplings to the baths and the dc electrical pumping are turned on, the magnon system is expected to approach a steady state in which spin and energy injected by the pumping process are precisely balanced by the spin and energy lost through dissipation. In this nonequilibrium steady state, the magnons should generally be characterized by a non-thermal distribution function, level broadening, etc., and their properties must be solved for in the presence of both drive and decay. To this end, the Keldysh path integral formalism<sup>20</sup> provides a systematic, straightforward way to trace out the bath degrees of freedom and obtain a reduced field theory for the magnons that takes the dissipative and nonequilibrium effects of the baths into account.

Central to the Keldysh functional integral formalism is the Keldysh action  $\mathcal{S}$ , which is obtained by time-evolving the system Lagrangian along the Schwinger-Keldysh time-loop contour, i.e., from an initial state in the infinite past  $t = t_0 = -\infty$  to the far future (i.e.,  $t = \infty$ ) and back to  $t_0$ . To reduce the time integrals to unidirectional ones, it is customary to double the degrees of freedom at every point in time by defining separate fields on the forward and the backward branches (labeled by + and -, respectively) of the time-loop contour. Following a standard procedure, we formulate  $\mathcal{S}$  in the RAK basis, where all bosonic fields on the forward and backward branches,  $\phi_q^+(t)$  and  $\phi_q^-(t)$ , are rotated to the ‘‘classical-quantum (c-q)’’ basis,  $\phi_q^c(t)$  and  $\phi_q^q(t)$ , and all fermionic fields on the contour,  $\psi_k^+(t)$  and  $\psi_k^-(t)$ , are rotated to the ‘‘1-2’’ basis,  $\psi_k^1(t)$  and  $\psi_k^2(t)$ .<sup>20</sup> In this basis, the causality structures of the bosonic ( $\hat{D}$ ) and fermionic ( $\hat{G}$ ) Green functions become

$$\hat{D} = \begin{pmatrix} D^K & D^R \\ D^A & 0 \end{pmatrix}, \quad \hat{G} = \begin{pmatrix} G^R & G^K \\ 0 & G^A \end{pmatrix}, \quad (3)$$

where  $R, A, K$  label the usual retarded, advanced and Keldysh components.

In the RAK basis, the Keldysh action for the magnon subsystem [corresponding to Eq. (2)] is given by

$$\begin{aligned} \mathcal{S}_F = & \sum_{\mathbf{q}} \int \frac{d\Omega}{2\pi} A_{\mathbf{q}}^\dagger(\Omega) \begin{pmatrix} D_{0\mathbf{q}}^K(\Omega) & D_{0\mathbf{q}}^R(\Omega) \\ D_{0\mathbf{q}}^A(\Omega) & 0 \end{pmatrix}^{-1} A_{\mathbf{q}}(\Omega) \\ & - \frac{1}{\mathcal{N}} \sum_{\{q_n\}} \int_{-\infty}^{\infty} dt V_{q_1 q_3} [a_{q_1}^{c*}(t) a_{q_2}^{c*}(t) a_{q_3}^c(t) a_{q_4}^q(t) \\ & + a_{q_1}^{q*}(t) a_{q_2}^{q*}(t) a_{q_3}^c(t) a_{q_4}^c(t) + c.c.] \delta_{q_1+q_2, q_3+q_4}, \quad (4) \end{aligned}$$

where  $A_{\mathbf{q}}^\dagger(\Omega) = (a_{\mathbf{q}}^{c*}(\Omega) \ a_{\mathbf{q}}^{q*}(\Omega))$  collects the classical and quantum components of the magnon field,  $a_{\mathbf{q}}(t) = \int (d\Omega/2\pi) a_{\mathbf{q}}(\Omega) e^{-i\Omega t}$ , and the components of the unperturbed magnon propagator matrix are given by

$$\begin{aligned} D_{0\mathbf{q}}^R(\Omega) &= \frac{1}{\Omega - (\varepsilon_{\mathbf{q}} + \mu_0)/\hbar + i\delta} = D_{0\mathbf{q}}^{A*}(\Omega), \\ D_{0\mathbf{q}}^K(\Omega) &= \coth\left(\frac{\hbar\Omega}{2k_B T}\right) [D_{0\mathbf{q}}^R(\Omega) - D_{0\mathbf{q}}^A(\Omega)], \end{aligned}$$

where  $T$  is the magnon temperature in the infinite past and  $\delta > 0$  is the usual infinitesimal parameter.

The Keldysh action for the  $i$ -th phonon bath and its coupling to the magnons at site  $i$  becomes

$$\mathcal{S}_i^B = \sum_{\alpha} \int \frac{d\Omega}{2\pi} B_{i,\alpha}^{\dagger}(\Omega) \begin{pmatrix} d_{\alpha}^K(\Omega) & d_{\alpha}^R(\Omega) \\ d_{\alpha}^A(\Omega) & 0 \end{pmatrix}^{-1} B_{i,\alpha}(\Omega) - \sum_{\alpha} \int \frac{d\Omega}{2\pi} [\kappa_{i,\alpha} B_{i,\alpha}^{\dagger}(\Omega) \hat{\tau}_x A_i(\Omega) + h.c.], \quad (5)$$

where  $B_{i,\alpha}^{\dagger}(\Omega) = (b_{i,\alpha}^{c*}(\Omega) b_{i,\alpha}^{q*}(\Omega))$ , once again, collects the classical and quantum components of the bath field and the bath Green functions read

$$d_{\alpha}^R(\Omega) = \frac{1}{\Omega - \Omega_{\alpha} + i\delta} = d_{\alpha}^{A*}(\Omega), \\ d_{\alpha}^K(\Omega) = -2\pi i \coth\left(\frac{\hbar\Omega}{2k_B T_B}\right) \delta(\Omega - \Omega_{\alpha});$$

we use  $\hat{\tau}_x$ ,  $\hat{\tau}_y$  and  $\hat{\tau}_z$  to denote Pauli matrices acting in Keldysh space.

Finally, the Keldysh action describing the  $i$ -th metallic bath and its coupling to the magnons is given by

$$\mathcal{S}_i^m = \sum_{k,\sigma} \int \frac{d\omega}{2\pi} \Psi_{i,k\sigma}^{\dagger}(\omega) \begin{pmatrix} g_{k\sigma}^R(\omega) & g_{k\sigma}^K(\omega) \\ 0 & g_{k\sigma}^A(\omega) \end{pmatrix}^{-1} \Psi_{i,k\sigma}(\omega) - \frac{\eta_i}{\sqrt{2}} \sum_{kk'} \int \frac{d\omega}{2\pi} \frac{d\omega'}{2\pi} [\Psi_{i,k\uparrow}^{\dagger}(\omega) a_i^c(\omega - \omega') \Psi_{i,k\downarrow}(\omega') + \Psi_{i,k\uparrow}^{\dagger}(\omega) a_i^q(\omega - \omega') \hat{\tau}_x \Psi_{i,k\downarrow}(\omega') + h.c.], \quad (6)$$

where  $\Psi_{i,k\sigma}^{\dagger}(\omega) = (\psi_{i,k\sigma}^{1*}(\omega) \psi_{i,k\sigma}^{2*}(\omega))$  collects the 1 and 2 components of the bath fermions, and the unperturbed bath fermion propagators are given by

$$g_k^R(\omega) = \frac{1}{\omega - \nu_k + i\delta} = g_k^{A*}(\omega) \\ g_{k\sigma}^K(\omega) = -2\pi i \tanh\left(\frac{\hbar\omega - \mu_{\sigma}}{2k_B T_F}\right) \delta(\omega - \nu_k).$$

The full Keldysh partition function can now be written as

$$Z = \int \frac{\mathcal{D}\{A_q(\Omega), B_{i,\alpha}(\Omega), \Psi_{i,k\sigma}(\omega)\}}{\text{Tr}\{\hat{\rho}_0\}} e^{i\mathcal{S}_F + i\sum_i(\mathcal{S}_i^B + \mathcal{S}_i^m)},$$

where  $\hat{\rho}_0$  is the density matrix at  $t = t_0$ .

## B. Tracing out the baths

We now integrate out the bath degrees of freedom in order to obtain an effective field theory for the active magnons. The assumption here is that the baths are infinite, so that they remain unperturbed from their equilibrium configuration even in the presence of the (possibly strongly nonequilibrium) magnon system. The effects of the infinite baths on the magnon subsystem can then be fully taken into account by

performing a functional integral over the baths. If the phonon baths are traced out, Eq. (5) is modified to

$$i\mathcal{S}_i^B \rightarrow -i \int \frac{d\Omega}{2\pi} A_i^{\dagger}(\Omega) \begin{pmatrix} 0 & \Sigma_i^A(\Omega) \\ \Sigma_i^R(\Omega) & \Sigma_i^K(\Omega) \end{pmatrix} A_i(\Omega),$$

where  $\Sigma_i^{R,A,K}(\Omega) = \sum_{\alpha} |\kappa_{i,\alpha}|^2 d_{\alpha}^{R,A,K}(\Omega)$  are the phonon-induced magnon self-energies. The retarded component may be written as

$$\Sigma_i^R(\Omega) = \int \frac{d\Omega'}{2\pi} \frac{2J_i^B(\Omega')}{\Omega - \Omega' + i\delta}, \quad (7)$$

where  $J_i^B(\Omega) = \pi \sum_{\alpha} |\kappa_{i,\alpha}|^2 \delta(\Omega - \Omega_{\alpha})$  is the spectral density of the  $i$ -th bath, and the Keldysh component reads

$$\Sigma_i^K(\omega) = -2iJ_i^B(\omega) \coth\left(\frac{\hbar\omega}{2k_B T_B}\right).$$

As Eq. (7) shows, the current formalism allows one to consider any functional form for the phonon spectral density  $J_i^B(\Omega)$ . Here, we proceed with an ohmic bath,

$$J_i^B(\Omega) = \alpha_i^B \Omega \frac{\Omega_c^2}{\Omega_c^2 + \Omega^2},$$

where we have introduced a Drude cutoff function with cutoff frequency  $\Omega_c$  and a site-dependent Gilbert damping parameter  $\alpha_i^B$ . In the low-frequency limit  $\Omega \ll \Omega_c$ , Eq. (7) reduces to

$$\Sigma_i^R(\Omega) = -\alpha_i^B (\Omega_c + i\Omega). \quad (8)$$

We therefore see that an ohmic bosonic bath here leads to the standard level broadening proportional to magnon frequency and thus to the familiar Gilbert damping phenomenology. The phonon baths here are sources of intrinsic Gilbert damping in the current formalism.

Integrating out the metallic degrees of freedom is relatively more complex compared to the bosonic case because the fermions and the magnons couple nonlinearly [see Eq. (6)]. Therefore, once the integrals over  $\Psi_{i,k\sigma}(\omega)$  are performed, the fermionic bath corrections to the effective magnon action arise at all even orders in  $\eta_i$  and renormalize the multi-magnon scattering vertices as well. At the gaussian order, the correction renormalizes the gaussian magnon action, i.e., the first term in Eq. (4),

$$i\mathcal{S}_i^{m(2)} = -i \int \frac{d\Omega}{2\pi} A_i^{\dagger}(\Omega) \begin{pmatrix} 0 & \Pi_i^A(\Omega) \\ \Pi_i^R(\Omega) & \Pi_i^K(\Omega) \end{pmatrix} A_i(\Omega),$$

where the components of the fermion-induced magnon self-energy matrix are given by

$$\Pi_i^R(\Omega) = -\frac{i|\eta_i|^2}{2} \sum_{kk'} \int \frac{d\omega'}{2\pi} [g_k^R(\Omega + \omega') g_{k'}^K(\omega') + g_{k\uparrow}^K(\Omega + \omega') g_{k'}^A(\omega')] = \Pi_i^{A*}(\Omega) \\ \Pi_i^K(\Omega) = -\frac{i|\eta_i|^2}{2} \sum_{kk'} \int \frac{d\omega'}{2\pi} [g_{k\uparrow}^K(\Omega + \omega') g_{k'}^K(\omega') + g_k^R(\Omega + \omega') g_{k'}^A(\omega') + g_k^A(\Omega + \omega') g_{k'}^R(\omega')].$$

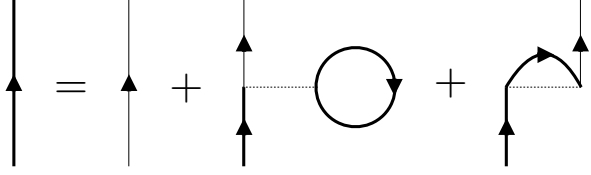


FIG. 2. Dyson equation for the full Green function in the self-consistent Hartree-Fock theory. Thin lines denote the noninteracting magnon propagator and heavy lines the full propagator. The dotted lines correspond to the interaction vertex  $V_{qq'}$ .

Performing the internal frequency integral, the self-energy functions become

$$\Pi_i^R(\Omega) = -\alpha_i^F(\Omega - \mu_s/\hbar) \quad (9)$$

$$\Pi_i^K(\Omega) = \coth\left(\frac{\hbar\Omega - \mu_s}{2k_B T_F}\right) [\Pi_i^R(\Omega) - \Pi_i^A(\Omega)], \quad (10)$$

where  $\alpha_i^F = \pi|\eta_i|^2\rho_0^2\hbar^2$  is the Gilbert damping arising from the metallic continuum and  $\rho_0$  is the bath fermion density of states at the Fermi level.

The next order correction comes at fourth order in  $\eta_i$  and renormalizes the quartic vertices in the magnon action [see the last two lines in Eq. (4)]. As shown in Appendix A, the fermionic bath not only generates corrections to the existing quartic coefficients but also generates new quartic terms with even powers of quantum fields  $a_q^q$ . However, the bath only generates dissipative vertices — quartic terms with purely imaginary coefficients — that are  $O[(\alpha_i^F)^2]$ , and, within the self-consistent Hartree-Fock approximation introduced below, they are expected to give subleading corrections to the dissipative effects already accounted for at the gaussian order [see Eqs. (9) and (10)]. We therefore ignore these metal-induced renormalizations of the quartic vertices in the remainder of the work.<sup>21</sup>

### III. SELF-CONSISTENT HARTREE-FOCK THEORY

We now discuss the properties of the driven, dissipative magnon subsystem in the normal (uncondensed) phase and discern the location of the BEC instability as a function of various system parameters such as the external magnetic field  $B$  and the bath temperatures  $T_B$  and  $T_F$ . This will be done by generalizing the self-consistent Hartree-Fock approach, used in equilibrium dilute imperfect Bose gases,<sup>22</sup> to the current nonequilibrium problem. For simplicity, we hereafter restrict our discussion to uniform magnon-bath coupling amplitudes, i.e.,  $\kappa_{i,\alpha} \rightarrow \kappa_\alpha$  and  $\eta_i \rightarrow \eta$ , though lifting this assumption is not expected to change the qualitative results presented below.

The Dyson equation for the full magnon Green function within the self-consistent Hartree-Fock approximation is diagrammatically shown in Fig. 2, where each magnon propagator has a Keldysh matrix structure consistent with Eq. (3). Each thin line represents the gaussian magnon propagator matrix [with components  $D_q^{R,A,K}(\Omega)$ ] that fully accounts for the nonequilibrium drive and dissipation. Its retarded component

can be easily read off from the reduced gaussian Keldysh action,

$$D_q^R(\Omega) = \frac{1}{\Omega - (\varepsilon_q + \mu_0)/\hbar - \Sigma^R(\Omega) - \Pi^R(\Omega)}, \quad (11)$$

where  $\Sigma^R(\Omega) = -\alpha_B\Omega$  and  $\Pi^R(\Omega) = -\alpha_F(\Omega - \mu_s/\hbar)$ , and  $\alpha_B$  and  $\alpha_F$  can now be interpreted as the (spatially uniform) Gilbert damping parameters arising from the phonon and metallic baths, respectively. In Eq. (11), we have dropped the constant real part in  $\Sigma^R$  [see Eq. (8)] by absorbing it into the bare magnon chemical potential  $\mu_0$ .

Similarly, the Keldysh component of the gaussian magnon propagator can be read off as  $D_q^K(\Omega) = [2N(\Omega) + 1][D_q^R(\Omega) - D_q^A(\Omega)]$ , where

$$N(\Omega) = \frac{1}{\alpha\Omega - \alpha_F\mu_s/\hbar} \times \left[ \frac{\alpha_B\Omega}{e^{\hbar\Omega/k_B T_B} - 1} + \frac{\alpha_F(\Omega - \mu_s/\hbar)}{e^{(\hbar\Omega - \mu_s)/k_B T_F} - 1} \right] \quad (12)$$

is the nonequilibrium magnon distribution function and  $\alpha = \alpha_B + \alpha_F$  is the total Gilbert damping parameter.

We see from Eq. (12) that the magnon distribution function, in general, has a nonthermal form in the presence of mismatched bath temperatures and/or electrical pumping. Even at zero pumping (i.e.,  $\mu_s = 0$ ),  $N(\Omega)$  is given by a linear combination of two Bose-Einstein distribution functions, one corresponding to the phonons equilibrated at temperature  $T_B$  and the other corresponding to the spin-1 particle-hole excitations in the metal equilibrated at temperature  $T_F$ , and they are weighted by the respective Gilbert damping parameters associated with each of the baths. This has important consequences on the finite temperature crossover behavior of the magnon system near the BEC critical line, as we later show in Sec. III C.

The steady-state non-thermal magnon distribution function obtained here contrasts with similar past studies of electrically pumped magnon BECs, in which magnons were assumed to be internally thermalized to the Bose-Einstein distribution function with a well-defined effective temperature and a chemical potential.<sup>11,23</sup>

#### A. Self-consistent solution

Within the self-consistent theory, the components of the Keldysh one-loop self-energy matrix are given by

$$\tilde{\Sigma}_q^R = -\frac{4}{\mathcal{N}} \frac{1}{\hbar} \sum_{q'} \int \frac{d\Omega}{2\pi} N(\Omega) (V_{qq'} + V_{q'q'}) \text{Im} \mathcal{D}_q^R(\Omega) = \tilde{\Sigma}_q^A,$$

where  $\mathcal{D}_q^R(\Omega)$  is the retarded component of the full self-consistent magnon propagator, and we find  $\tilde{\Sigma}_q^K = 0$ . This then leads to a self-consistent magnon spectrum given by

$$\tilde{\varepsilon}_q + \mu = \varepsilon_q + \mu_0 - \frac{4}{\mathcal{N}} \sum_{q'} \int \frac{d\Omega}{2\pi} N(\Omega) (V_{qq'} + V_{q'q'}) \text{Im} \{ \mathcal{D}_q^R(\Omega) \}, \quad (13)$$

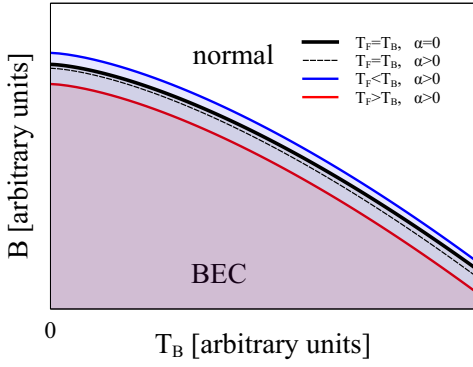


FIG. 3. (color online) Critical lines separating the BEC phase from the normal phase at zero electrical pumping,  $\mu_s = 0$ . The phase diagram is spanned by the magnetic field  $B$  and phonon temperature  $T_B$ . The solid black line corresponds to the equilibrium, isolated limit with  $T_B = T_F$  and  $\alpha = 0$ . For  $\alpha = 0.1$ , the dashed line obtains, indicating that the BEC region is shrunk by dissipation. The red (blue) line corresponds to the critical line with  $T_F > T_B$  ( $T_B < T_F$ ); here, we have chosen  $\alpha_B = \alpha_F$ .

where the full retarded magnon propagator above is defined with the renormalized spectrum  $\tilde{\varepsilon}_q$  and chemical potential  $\mu$ , i.e.,

$$\mathcal{D}_q^R(\Omega) = \frac{1}{\Omega - (\tilde{\varepsilon}_q + \mu)/\hbar + i\alpha\Omega - i\alpha_F\mu_s/\hbar}. \quad (14)$$

The magnon spectral function,  $\mathcal{A}_q(\Omega) = -2\text{Im}\mathcal{D}_q^R(\Omega)$ , is strongly peaked at  $q \sim [2(\hbar\Omega - \mu)/J_0S\xi_J^2]^{1/2}$ . Therefore, contributions to the integral coming from large wavevectors  $q' \sim \xi_J^{-1}$  in Eq. (13) (assuming that the spatial range of the exchange constant is on the order of a few lattice constants) is exponentially suppressed by  $N(\Omega)$  as long as  $J_0S/k_B T_B, J_0S/k_B T_F \gg 1$ , which is almost always true. The last term in Eq. (13) can then be evaluated by setting  $q' = 0$ . Now, expanding  $V_{q0}$  to quartic order in  $q\xi_J \ll 1$  and  $q\xi_K \ll 1$ , the self-consistent equation becomes

$$\tilde{\varepsilon}_q + \mu = \varepsilon_q + \mu_0 + 2n[(K_0 + J_0(4\lambda - 1)) - \frac{K_0(q\xi_K)^2 + J_0(q\xi_J)^2(2\lambda - 1)}{2}]n, \quad (15)$$

where

$$n = -\frac{2}{\mathcal{N}} \sum_q \int \frac{d\Omega}{2\pi} N(\Omega) \text{Im}\{\mathcal{D}_q^R(\Omega)\}$$

is the magnon number per lattice site. The second term on the right hand side of Eq. (15) renormalizes the effective magnon mass. However, this correction remains small in the dilute magnon limit, i.e.,  $n/S \ll 1$ . We therefore ignore this correction as well and finally arrive at the self-consistent equation for the magnon chemical potential (i.e., the magnon gap),

$$\mu = \mu_0 + 2n[K_0 + J_0(4\lambda - 1)]. \quad (16)$$

## B. BEC critical line

We now construct a two-dimensional phase diagram for the magnon system spanned by the phonon temperature  $T_B$  and external magnetic field  $B$ . We define the equilibrium limit as  $T_B = T_F \equiv T$  and  $\mu_s = 0$ , in which the magnons are thermalized at temperature  $T$  and then study the departures from equilibrium systematically by introducing  $T_F \neq T_B$  and  $\mu_s > 0$ .

In the absence of spin accumulation in the metal, i.e.,  $\mu_s = 0$ , the BEC critical line [defined by  $\mu = 0$  in Eq. (16)] translates to the following critical magnetic field

$$\hbar\gamma B_c = S K_0 - \Gamma_\alpha c \left[ \frac{\alpha_B}{\alpha} T_B^{3/2} + \frac{\alpha_F}{\alpha} T_F^{3/2} \right], \quad (17)$$

where

$$c = [K_0 + J_0(4\lambda - 1)] \frac{v_s \zeta_{3/2}(1)}{\sqrt{2} \xi_J^3} \left( \frac{k_B}{\pi J_0 S} \right)^{3/2}.$$

Here,  $\zeta_{3/2}(x)$  is the polylog function,  $v_s$  is the volume occupied by each atomic spin, and  $\Gamma_\alpha = (1 + \alpha^2)^{1/4} \cos[(\tan^{-1} \alpha)/2]$  is a prefactor that arises due to dissipation. In the equilibrium and isolated limits, i.e.,  $T_B = T_F$  and  $\alpha = 0$ , we have  $\Gamma_\alpha = 1$  and Eq. (17) reduces to the well-known BEC critical line for a dilute Bose gas (see solid black line in Fig. 3).<sup>18,22</sup> If we then introduce Gilbert damping  $\alpha > 0$  (while still keeping  $T_F = T_B$ ), the critical line is modified to the dashed line; we find that dissipation, as expected, leads to the shrinking of the BEC phase region.

The two colored lines give the critical lines for mismatched bath temperatures,  $T_F \neq T_B$ , the red and blue lines corresponding to  $T_F > T_B$  and  $T_F < T_B$ , respectively. We find that raising (lowering) the fermion bath temperature above (below) the phonon temperature generally destabilizes (stabilizes) the BEC phase. In the absence of electrical pumping  $\mu_s = 0$ , our model therefore predicts that triggering a steady state magnon BEC with a *positive* temperature difference between the metal and the phonons ( $T_F - T_B > 0$ , i.e., magnon BEC via spin Seebeck mechanism alone) is not possible.

The reason for this claim can be understood as follows. Our theoretical analysis in Sec. II shows that once the phonon and metallic baths are integrated out, magnon distribution function Eq. (12) is no longer thermal with a well-defined temperature and chemical potential, but is defined by the distribution functions of both baths. The magnon distribution function therefore “floats” (i.e., adjusts) according to the thermal distribution functions of the surrounding baths. In this sense, it would be reasonable to expect that realizing magnon BEC by heating the metal is impossible because that will always heat up the magnon system and hinder condensation.

Electrically-pumped BEC of magnons in a setup very similar to Fig. 1 was studied recently in Ref. 11 by assuming that magnons remain internally thermalized with an effective temperature and chemical potential. In the so-called “floating temperature” regime, the work obtains the effective magnon temperature by balancing the spin/energy transfer across the metal-magnet interface and loss to the phonon bath. In this regime, the work shows that raising (lowering) the metal tem-



perature above (below) the phonon temperature tends to hinder (facilitate) magnon condensation, and therefore shows some level of consistency with our findings.

### C. Finite-temperature crossovers

The presence of two bath temperatures endows the current system with a richer finite temperature crossover behavior compared to the standard critical Bose gas in equilibrium.<sup>18</sup> In this section, we still keep  $\mu_s = 0$  and study the effects of the two bath temperatures in the vicinity of the  $T_B = T_F = 0$  quantum critical point located at  $\mu_0 = 0$ . For weak dissipation,  $\alpha_B, \alpha_F \ll 1$ , we find that the effects of the baths on the magnon density of states  $\rho_m(\Omega)$  are very weak, so we approximate  $\rho_m$  with its expression in the isolated limit, i.e.,

$$\rho_m(\Omega) = -\frac{1}{\hbar} \sum_q \text{Im} \mathcal{D}_q^R(\Omega) \approx \frac{\mathcal{V} \sqrt{\hbar\Omega - \mu\theta(\hbar\Omega - \mu)}}{\sqrt{2\pi}(J_0 S \xi^2)^{3/2}},$$

where  $\mathcal{V}$  is the volume of the ferromagnet. Then the self-consistent condition for the magnon gap  $\mu$  becomes [c.f. Eq. (16)]

$$\mu = \mu_0 + \frac{\alpha_B}{\alpha} \left[ \frac{\zeta_{3/2}(e^{-\mu/k_B T_B})}{\zeta_{3/2}(1)} \right] c T_B^{3/2} + \frac{\alpha_F}{\alpha} \left[ \frac{\zeta_{3/2}(e^{-\mu/k_B T_F})}{\zeta_{3/2}(1)} \right] c T_F^{3/2}.$$

We note that  $c T_B^{3/2}/k_B T_B \ll 1$  and  $c T_F^{3/2}/k_B T_F \ll 1$  hold as long as both bath temperatures are much less than the exchange scale, i.e.,  $T_B, T_F \ll J_0/k_B$ , which is almost always true. Then the magnon gap can be quite easily solved by iteration in nine different regimes as shown in Fig. 4. The gap  $\mu$  is also directly related to the correlation length  $\xi$  of the superfluid order parameter fluctuations via  $\xi^{-2} \propto \mu$ , so Fig. 4 summarizes how the correlation length of the critical fluctuations, which diverges right at the critical line, is cutoff by departures from the critical line.

The familiar finite temperature crossover behavior of the (inverse square of the) correlation length for an equilibrium dilute Bose gas<sup>18</sup> can essentially be reproduced by setting  $\alpha_F = 0$  in the current discussion and varying the phonon temperature. The three regimes that arise in this case are enclosed in the thick red box in Fig. 4. At low temperatures  $T_B \ll \mu_0/k_B$  (shaded in blue), the correlation length is essentially cutoff by the bare gap  $\mu_0$  and its  $T$ -dependent corrections are exponentially small. In this regime, the inter-particle spacing between the magnons is much larger than the thermal de Broglie wavelength and the the magnon density is exponentially small. In the intermediate temperature regime  $\mu_0/k_B \ll T_B \ll (\mu_0/c)^{2/3}$  (shaded in green),  $\xi^{-2}$  is still dominated by  $\mu_0$ , however, the subleading correction now possesses a power-law form in contrast to the exponential form obtained in the low-temperature regime. In this regime, the magnon density scales with temperature as  $T_B^{3/2}$  and the inter-particle spacing becomes of order the de Broglie wavelength. Finally, in the high-temperature regime  $T_B \gg (\mu_0/c)^{2/3}$  (shaded in red), the correlation length is cutoff by temperature and one finds  $\xi \sim T_B^{-3/4}$ .

	IIIF1 $\frac{\alpha_F c}{\alpha} T_F^{3/2}$	IIIF2 $\frac{\alpha_F c}{\alpha} T_F^{3/2}$	III $\frac{\alpha_B c}{\alpha} T_B^{3/2} + \frac{\alpha_F c}{\alpha} T_F^{3/2}$
$T_F$ $(\alpha\mu_0/\alpha_F c)^{2/3}$	IIF $\mu_0 + \frac{\alpha_F c}{\alpha} T_F^{3/2}$	II $\mu_0 + \frac{\alpha_B c}{\alpha} T_B^{3/2} + \frac{\alpha_F c}{\alpha} T_F^{3/2}$	IIIB2 $\frac{\alpha_B c}{\alpha} T_B^{3/2}$
$\mu_0/k_B$	I $\mu_0$	IIB $\mu_0 + \frac{\alpha_B c}{\alpha} T_B^{3/2}$	IIIB1 $\frac{\alpha_B c}{\alpha} T_B^{3/2}$
		$\mu_0/k_B$	$T_B$ $(\alpha\mu_0/\alpha_B c)^{2/3}$

FIG. 4. (color online) Approximate expressions for the (inverse square of the) correlation length  $\xi^{-2}$  for  $\mu_s = 0$ . The columns separate the low, intermediate and high temperature regimes with respect to the phonon temperature, while the rows separate the three regimes with respect to the metal temperature. The three finite-temperature regimes familiar from the equilibrium dilute Bose gas are enclosed by the thick red box.

If we now re-introduce the fermionic bath (i.e.,  $\alpha_F > 0$ ), each of the three regimes mentioned above is further subdivided into three sub-regimes depending on the magnitude of the metal temperature  $T_F$  (see Fig. 4): the bottom row corresponds to its low temperature regime with  $T_F \ll \mu_0/k_B$ , the middle row to intermediate temperatures  $\mu_0/k_B \ll T_F \ll (\alpha\mu_0/\alpha_F c)^{2/3}$  and the top row to the high temperature regime  $T_F \gg (\alpha\mu_0/\alpha_F c)^{2/3}$ . We see that the corrections to the magnon gap coming from  $T_F$  are exponentially small in the low temperature regime and so  $T_F$  essentially does not enter the expression for the correlation length (see the bottom row). However, in analogy with  $T_B$ , the metal temperature becomes increasingly effective in cutting off the correlation length as it increases, and once the high temperature regime is reached (see the top row), the correlation length essentially becomes defined by  $T_F$  unless the phonon temperature  $T_B$  is also in the high temperature regime (i.e., the top right corner).

### D. BEC instability due to electrical pumping

Let us now reinstate the electrical pumping  $\mu_s$ . As one increases the nonequilibrium spin accumulation  $\mu_s$  from zero in the normal phase, the instability of the magnon system is signaled once the frequency  $\mu/\hbar$  corresponding to the excitations at the bottom of the band obeys  $\text{Im}\{\mathcal{D}_q^{R-1}(\mu/\hbar)\} = 0$ , i.e.,

$$\mu_s^c = \left(1 + \frac{\alpha_B}{\alpha_F}\right) \mu. \quad (18)$$

If  $\mu_s$  is increased beyond this point, the imaginary parts of the small- $q$  poles become positive and fluctuations in the system

grow in time, thus signaling an instability.<sup>24</sup>

Comparing Eq. (14) and Eq. (12), we see that the condition Eq. (18) signals a divergence in the magnon distribution function  $N(\Omega)$ . However, the nonequilibrium drive  $\mu_s$  has relatively little effect on the magnon gap  $\mu$  as we now show. We focus on the limit of equal bath temperatures, i.e.,  $T_B = T_F \equiv T$ , for simplicity. In this case, the self-consistent condition for the magnon gap Eq. (16) reduces to

$$\mu = \mu_0 + \left[ \mathfrak{M}_B \left( \frac{\mu}{k_B T}, \frac{\mu_s}{k_B T} \right) + \mathfrak{M}_F \left( \frac{\mu}{k_B T}, \frac{\mu_s}{k_B T} \right) \right] c T^{3/2}, \quad (19)$$

where the two dimensionless functions are given by

$$\mathfrak{M}_B(x, y) = \frac{2\alpha_B}{\alpha \sqrt{\pi} \zeta_{3/2}(1)} \int_0^\infty \frac{ds \sqrt{s}}{s + x - (\alpha_F/\alpha)y} \frac{s + x}{e^{s+x} - 1},$$

$$\mathfrak{M}_F(x, y) = \frac{2\alpha_F}{\alpha \sqrt{\pi} \zeta_{3/2}(1)} \int_0^\infty \frac{ds \sqrt{s}}{s + x - (\alpha_F/\alpha)y} \frac{s + x - y}{e^{s+x-y} - 1}.$$

If we solve Eq. (19) self-consistently for  $\mu$ , we find that the electrical pumping  $\mu_s$  only gives negligible corrections to the magnon gap expressions already obtained in the  $\mu_s = 0$  limit (c.f. Fig. 4). In particular, as long as  $T \ll (\alpha\mu_0/\alpha_B c)^{2/3}$  and  $T \ll (\alpha\mu_0/\alpha_F c)^{2/3}$  (i.e., regimes I and II), the last two terms in Eq. (19) remain small compared to the first term for all  $\mu_s$ , therefore,  $\mu \approx \mu_0$  still holds in those regimes. At high temperatures, i.e.,  $T \gg (\alpha\mu_0/\alpha_B c)^{2/3}$  or  $T \gg (\alpha\mu_0/\alpha_F c)^{2/3}$ , we obtain  $\mu \sim T^{3/2}$  since  $\mathfrak{M}_{B,F}(0 \leq x \ll 1, 0 \leq y \ll 1) \approx \text{const.} \sim \mathcal{O}(1)$ .

#### IV. SPIN CONDUCTIVITY

Finite temperature crossover behavior exhibited by the magnon gap (see Fig. 4) entails a corresponding crossover behavior in the magnon spin conductivity. Here, we use the Kubo formalism to compute the spin conductivity of this magnon gas within the normal phase and the Hartree-Fock approximation as a function of the bath temperatures  $T_B$  and  $T_F$  and the magnetic field  $\mu_0$ . We later investigate the effects of finite electrical pumping  $\mu_s > 0$ .

Spin conductivity can be obtained by looking at the response of the magnons to an external magnetic field  $B(\mathbf{x}, t)$ ; here, we focus only on the spin current polarized along the  $z$  axis, which is the conserved component. The relevant (time-dependent) perturbation can then be written as

$$H'(t) = \hbar\gamma \int d^3\mathbf{x} B(\mathbf{x}, t) a^\dagger(\mathbf{x}) a(\mathbf{x}),$$

where  $a(\mathbf{x}) = a_i/v_s^{1/2}$  is the continuum magnon field operator. Assuming that the magnetic field has a uniform gradient only along the  $x$  axis, the resulting spin current  $J(\mathbf{x}, t)$  flowing along the same axis, within linear-response, reads<sup>25–27</sup>

$$J(\mathbf{x}, t) = \hbar\gamma \int d^3\mathbf{x}' \int dt' \chi(\mathbf{x} - \mathbf{x}', t - t') B(\mathbf{x}', t'),$$

where the susceptibility is defined as

$$\chi(\mathbf{x} - \mathbf{x}', t - t') = -\frac{i}{\hbar} \theta(t - t') \langle [J(\mathbf{x}, t), \varrho(\mathbf{x}', t')] \rangle_{\text{HF}}, \quad (20)$$

$\varrho(\mathbf{x}, t) = a^\dagger(\mathbf{x}, t) a(\mathbf{x}, t)$  is the magnon density operator and  $j(\mathbf{x}, t) = i(J_0 S \xi_J^2/2) [\partial_x a^\dagger(\mathbf{x})] a(\mathbf{x}) + h.c.$  is the magnon spin current operator. The spin conductivity  $\sigma$  is then defined as the constant of proportionality between the negative gradient in the magnetic field and the spin current that flows in response to it, i.e.,  $J_q(\omega) = \sigma(\mathbf{q}, \omega) (-i q_x) \hbar \gamma B_q(\omega)$ , where  $\sigma(\mathbf{q}, \omega) = (-i q_x)^{-1} \chi(\mathbf{q}, \omega)$ . Within the Hartree-Fock approximation and in the uniform limit, spin conductivity can then be evaluated straightforwardly by first computing the susceptibility Eq. (20), and we obtain

$$\sigma(\mathbf{q} \rightarrow 0, \omega) = -\frac{1}{\gamma} \left( \frac{J_0 S \xi_J^2}{2\hbar} \right)^2 \frac{P(\omega) - P(0)}{\omega},$$

where

$$P(\omega) = \int \frac{d\Omega}{2\pi} \sum_k (2k_x)^2 \left[ \mathcal{D}_k^R(\Omega + \omega) \mathcal{D}_k^<(\Omega) + \mathcal{D}_k^<(\Omega + \omega) \mathcal{D}_k^A(\Omega) \right],$$

and  $\mathcal{D}_k^<(\Omega) = -iN(\Omega)\mathcal{A}_k(\Omega)$  is the lesser Green function. Finally, taking the  $\omega \rightarrow 0$  limit, the dc spin conductivity  $\sigma_0$  is given by

$$\sigma_0 = -\frac{2}{3} \left( \frac{J_0 S \xi_J^2}{2\hbar} \right)^2 \int \frac{d\Omega}{2\pi} \int \frac{d^3\mathbf{k}}{(2\pi)^3} \partial_\Omega N(\Omega) k^2 \mathcal{A}_k^2(\Omega). \quad (21)$$

#### A. Finite-temperature crossovers

Let us first fix  $\mu_s = 0$  and explore the behavior of the dc spin conductivity in the various finite temperature regimes considered in Sec. III C. Both the phonon bath and the metal contribute to the thermal population of magnons inside the ferromagnet. Therefore, the total spin conductivity contains two contributions  $\sigma_0 = (\alpha_B/\alpha)\sigma_B + (\alpha_F/\alpha)\sigma_F$ , where  $\sigma_B$  ( $\sigma_F$ ) is the contribution arising from the phonon (metallic) bath. Once again, evaluating Eq. (21) in the limit of weak damping  $\alpha_B, \alpha_F \ll 1$ ,  $\sigma_0$  can be well approximated by

$$\sigma_{B,F} \approx \frac{1}{24\pi^2 \alpha} \sqrt{\frac{2k_B T_{B,F}}{J_0 S \xi_J^2}} \mathfrak{E} \left( \frac{\mu}{k_B T_{B,F}} \right),$$

where the function  $\mathfrak{E}(y)$  has the asymptotic behavior

$$\mathfrak{E}(y) \approx \begin{cases} \frac{3\sqrt{\pi}}{4} \frac{e^{-y}}{y}, & y \gg 1 \\ \frac{3\pi}{2} \frac{1}{\sqrt{y}}, & y \ll 1 \end{cases}.$$

In the low temperature regime  $T_B, T_F \ll \mu_0/k_B$ , each bath generates very few thermal magnons in the ferromagnet and the conductivity becomes exponentially suppressed. In this limit,  $\mu \approx \mu_0$  and we obtain

$$\sigma_{B,F} \approx \frac{\sqrt{2}}{32\alpha \xi_J} \left( \frac{J_0 S}{\mu_0} \right) \left( \frac{k_B T_{B,F}}{\pi J_0 S} \right)^{3/2} e^{-\mu_0/k_B T_{B,F}}. \quad (22)$$



TABLE I. Magnon spin conductivities in the various finite temperature regimes introduced in Fig. 4. Recall that  $\mu_0 = \hbar\gamma B - SK_0$ . See Fig. 4 for the labeling convention of the various temperature regimes.

Regime	$\sigma_0$
I	$\propto \alpha_B \frac{T_B^{3/2}}{\mu_0} e^{-\mu_0/k_B T_B} + \alpha_F \frac{T_F^{3/2}}{\mu_0} e^{-\mu_0/k_B T_F}$
II	$\propto \alpha_B \frac{T_B}{\sqrt{\mu_0}} + \alpha_F \frac{T_F}{\sqrt{\mu_0}}$
IIB	$\propto \frac{T_B}{\sqrt{\mu_0}}$
IIIF	$\propto \frac{T_F}{\sqrt{\mu_0}}$
III	$\propto \frac{\alpha_B T_B + \alpha_F T_F}{\sqrt{\alpha_B^3 T_B^{3/2} + \alpha_F T_F^{3/2}}}$
IIIB1 & IIIB2	$\propto T_B^{1/4}$
IIIF1 & IIIF2	$\propto T_F^{1/4}$

When the bath temperatures are in the intermediate to high temperature regimes  $T_B, T_F \gg \mu_0/k_B$ , the dimensionless function  $\mathfrak{S}(y)$  crosses over to the other asymptotic regime, and we obtain

$$\sigma_{B,F} \approx \frac{\sqrt{2}}{16\alpha\xi_J} \sqrt{\frac{J_0 S}{\mu}} \left( \frac{k_B T_{B,F}}{\pi J_0 S} \right),$$

where the expressions for  $\mu$  are presented in Sec. III C. Based on these results, we summarize the temperature and magnetic field dependences of  $\sigma_0$  in Table I. The results in the table hold for arbitrary  $\alpha_B$  and  $\alpha_F$  as long as they are of similar order. The regime labels correspond to those introduced in Fig. 4.

### B. BEC instability due to electrical pumping

In the presence of electrical pumping and as  $\mu_s$  approaches the BEC instability point  $\mu_s^c$  [see Eq. (18)], we find that spin conductivity diverges algebraically. The relevant exponent can be found straightforwardly by evaluating Eq. (21) now with  $\mu_s \neq 0$ . Here, we fix the magnon gap (which is essentially  $\mu_s$ -independent as discussed in Sec. III D) to some finite positive value  $\mu > 0$  and sweep  $\mu_s$  toward  $\mu_s^c$ ; we also assume that the bath temperatures are also fixed and do not change as electrical pumping is increased to the instability point. In the limit of weak damping  $\alpha_B, \alpha_F \ll 1$ , we find

$$\sigma_0 \approx \frac{1}{6\pi^2} \sqrt{\frac{2}{J_0 S \xi_J^2}} \int_{\mu/\hbar}^{\infty} d\Omega N(\Omega) \frac{\partial}{\partial \Omega} \frac{(\hbar\Omega - \mu)^{3/2}}{\alpha\hbar\Omega - \alpha_F \mu_s},$$

which, via power counting, we find to diverge as  $(\mu_s^c - \mu_s)^{-1/2}$  as  $\mu_s \rightarrow \mu_s^c$ .

## V. DISCUSSION

Spin conductivity predictions in Sec. IV can be experimentally verified using a two-terminal spin transport setup very similar to the devices studied in, e.g., Refs. 12 and 28. The setup of interest is shown in Fig. 5. The magnons are injected

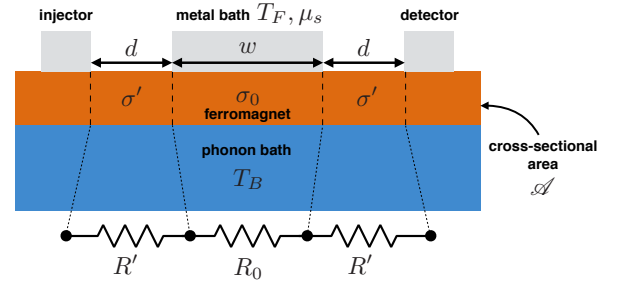


FIG. 5. (color online) A possible device for measuring spin conductivity. Magnons are injected into the ferromagnet by the injector metal via spin Hall effect in the metal, and magnon conductivity is quantified by electrically measuring the magnon density underneath the detector metal. The central metal bath is thermalized at temperature  $T_F$  and may possess a spin-Hall generated nonequilibrium spin accumulation  $\mu_s$  that can pump spin into the ferromagnetic region directly underneath it. The entire ferromagnet is coupled to a phonon bath at temperature  $T_B$ . The three ferromagnetic regions in between the injector and detector metals can be modeled as three resistances in series, as shown at the bottom of the figure.

at the injector metal via the spin Hall effect in the metal, and the magnon conductivity is quantified by electrically measuring the magnon density underneath the detector metal. The central metal bath is thermalized at temperature  $T_F$  and the nonequilibrium spin accumulation  $\mu_s$  generated via the spin Hall effect in the metal can inject spin current into the region of the ferromagnet directly beneath the metal. The entire ferromagnet is coupled to a phonon bath at temperature  $T_B$ .

Following Ref. 12, we characterize the region in the ferromagnet in between the injector and detector metals (with length  $2d + w$ ) using a series resistor model (see Fig. 5). Given that the ferromagnetic cross-sectional area is  $\mathcal{A}$  and that the conductivities in the three regions from left to right are  $\sigma'$ ,  $\sigma_0$  and  $\sigma'$ , respectively, the total spin resistance  $R = 1/G$  of the region should be given by

$$R = \frac{1}{G} = \frac{2d}{\sigma' \mathcal{A}} + \frac{w}{\sigma_0 \mathcal{A}} \equiv 2R' + R_0.$$

The spin conductivity  $\sigma'$  for the region outside of the central region (beneath the metal bath) can be obtained from  $\sigma_0$  computed in Sec. IV by setting  $\alpha_F = 0$ , i.e.,

$$\frac{1}{R'} = \frac{\sigma_0 \mathcal{A}}{d} \Big|_{\alpha_F=0}.$$

The first set of experiments can be performed in the absence of electrical pumping, i.e.,  $\mu_s = 0$ , maintaining the temperatures of the two baths equal, i.e.,  $T_F = T_B = T$ , and sweeping  $T$ . If the external field is fixed at some value with  $\mu_0 = \hbar\gamma B - SK_0 > 0$ , the gradual increasing of  $T$  from small ( $T \ll \mu_0/k_B$ ) to large [ $T \gg T_{\max} \equiv \max\{(\alpha_B \mu_0/\alpha_C)^{2/3}, (\alpha_F \mu_0/\alpha_C)^{2/3}\}$ ] values will then allow one to probe the finite temperature crossover behavior of the spin conductivity. The expected crossover behavior is shown in Fig. 6. At small temperatures  $T \ll \mu_0/k_B$  (regime I), the spin conductivities  $\sigma', \sigma_0$  both scale as  $T^{3/2} e^{-\mu_0/k_B T}$  [see Eq. (22)] as shown by the blue line in

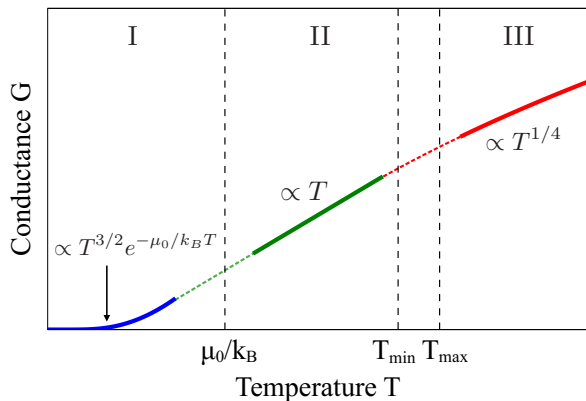


FIG. 6. (color online) The total spin conductance for the magnon gas located in between the injector and detector metals for a fixed magnetic field  $\mu_0$  and for  $\mu_s = 0$ . We assume here that  $T_B = T_F \equiv T$ . The conductance traverses through three regimes as the bath temperature  $T$  increased from the low temperature regime  $T \ll \mu_0/k_B$  (regime I), through the intermediate regime  $\mu_0/k_B \ll T \ll T_{\min}$  (regime II), and finally to the high temperature regime  $T \gg T_{\max}$  (regime III). Here,  $T_{\min} \equiv \min\{(\alpha_B \mu_0/\alpha c)^{2/3}, (\alpha_F \mu_0/\alpha c)^{2/3}\}$  and  $T_{\max} \equiv \max\{(\alpha_B \mu_0/\alpha c)^{2/3}, (\alpha_F \mu_0/\alpha c)^{2/3}\}$ .

Fig. 6. As the temperature increases into the intermediate and high temperature regimes (see regimes II and III in Fig. 6), the spin conductivities (and hence the spin conductance) exhibit power law behavior. In the intermediate temperature regime  $\mu_0/k_B \ll T \ll T_{\min} \equiv \min\{(\alpha_B \mu_0/\alpha c)^{2/3}, (\alpha_F \mu_0/\alpha c)^{2/3}\}$ ,  $\sigma'$  and  $\sigma_0$  both scale linearly in  $T$ , while the behavior crosses over to  $T^{1/4}$  in the high temperature regime  $T \gg T_{\max}$ .

We now include the effect of the electrical pumping  $\mu_s$ . Here, we fix both bath temperatures to  $T$ , fix the external magnetic field as well such that  $\mu_0$  is constant, but sweep the nonequilibrium spin accumulation  $\mu_s$  toward  $\mu_s^c$ . The spin resistance outside of the spin injection region is then fixed to a value  $R'$  that is independent of  $\mu_s$ , but  $1/R_0 = \sigma_0 \mathcal{A}/w$  exhibits a diverging behavior as already shown in Sec. IV B. We plot the spin resistance  $R$  (in units of  $R'$ ) as a function of  $\mu_s$  in Fig. 7 for  $d = w$  and for various ratios of  $\mu/k_B T = 0.01, 0.1, 1, 10$ . We find that as  $\mu_s$  approaches the critical value, the resistance in the central region (beneath the metal bath) goes to zero and so the total resistance converges from above to  $2R'$ . Evidently, the expected square root rise of the curves for  $\mu_s \lesssim \mu_s^c$  is most apparent at relative high temperatures, e.g.,  $\mu/k_B T \sim 0.01$ . Here, we have chosen  $\alpha_B = \alpha_F = 0.01$ . The y-intercepts of all the curves generally move up (down) when  $\alpha_F$  is increased above (decreased below)  $\alpha_B$ ; while the intercepts shift, the qualitative shapes of the curves do not change even when  $\alpha_F$  deviates from  $\alpha_B$ .

## VI. CONCLUSION

We present a microscopic theory based on the Keldysh path integral formalism to study a magnon gas in contact with a phonon bath and a metallic bath capable of dc electrical spin injection. For mismatched bath temperatures and/or finite dc

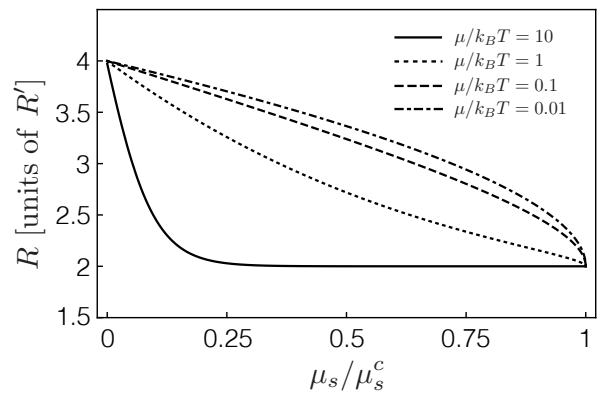


FIG. 7. Spin resistance  $R$  as a function of electrical pumping  $\mu_s$  for various values of  $\mu/k_B T$ , where  $T_B = T_F \equiv T$ . Here,  $R$  is plotted in units of  $R'$  and we have used  $\alpha_B = \alpha_F = 0.01$  and  $d = w$ .

electrical pumping, the magnon system converges to a non-thermal steady state in which the distribution function is given by a nontrivial superposition of the bath distribution functions. Focusing exclusively on the normal (uncondensed) phase, we analyze the finite temperature crossover behavior of the correlation length associated with the superfluid order parameter fluctuations as a function of both the phonon and metallic bath temperatures, and find that while the correlation length is essentially defined by the nonthermal control parameter (i.e., the external magnetic field) at low bath temperatures, any one of the bath temperatures can cut off the correlation length when it is raised to a sufficiently high value. Motivated by recent spin transport measurements on a magnon gas close to BEC instability,<sup>12</sup> we compute the linear spin conductivity for arbitrary bath temperatures and electrical pumping strengths, and show that the finite temperature crossover behavior in the correlation length directly leads to nontrivial dependences of the spin conductivity on the bath temperatures. In the presence of pumping, we find an inverse square-root divergence in the spin conductivity as the pumping strength approaches the threshold value for BEC instability. Two-terminal spin transport setups capable of verifying our predictions are presented.

Recently, the stability criteria for a magnon gas in contact with a metallic bath and in the presence of electrical spin current injection were studied using the Keldysh path integral formalism.<sup>17</sup> While the microscopic Keldysh formulation was applied to the normal phase in both Ref. 17 and here, extending this approach for spin transport analysis in the condensed phase is an interesting future direction. Furthermore, a full microscopic derivation of the *nonlinear* dynamics involving both the condensate and the thermal cloud in an electrically pumped magnon system (e.g., as studied in Ref. 11) using the Keldysh formulation is also an interesting open problem.

## ACKNOWLEDGMENTS

The author would like to thank Yaroslav Tserkovnyak for a helpful correspondence. This research was supported by Research Foundation CUNY Project # 90922-07 10.

## Appendix A: Quartic vertices generated by the metal baths

In this appendix, we compute the corrections to the quartic coefficients arising from integrating out the fermionic degrees of freedom. At fourth order in  $\eta_i$ , we obtain the following correction to the quartic terms in  $\mathcal{S}_F$  [i.e., the last two terms in Eq. (4)]

$$\begin{aligned} \iota \mathcal{S}_i^{m(4)} = & -\frac{|\eta_i|^4}{8} \sum_{\{k_i\}} \int \frac{d\omega}{2\pi} \int \frac{d\omega'}{2\pi} \int \frac{d\omega''}{2\pi} \int \frac{d\omega'''}{2\pi} \\ & \times \text{Tr} \left[ \hat{g}_{k_{1\uparrow}}(\omega + \omega' + \omega'' - \omega''') \hat{A}_i(\omega) \hat{g}_{k_{2\downarrow}}(\omega' + \omega'' - \omega''') \right. \\ & \left. \times \hat{A}_i^*(\omega'') \hat{g}_{\uparrow}(\omega' + \omega''') \hat{A}_i(\omega') \hat{g}_{k_{3\downarrow}}(\omega''') \hat{A}_i^*(\omega + \omega' - \omega'') \right], \end{aligned}$$

where

$$\hat{g}_{k\sigma}(\omega) = \begin{pmatrix} g_{k\sigma}^R(\omega) & g_{k\sigma}^K(\omega) \\ 0 & g_{k\sigma}^A(\omega) \end{pmatrix}, \quad \hat{A}_i(\omega) = \begin{pmatrix} a_i^c(\omega) & a_i^q(\omega) \\ a_i^q(\omega) & a_i^c(\omega) \end{pmatrix}.$$

Since we expect the energies of the magnons to be much smaller than the Fermi energy, we approximate the above expression by setting  $\omega' = \omega'' = \omega = 0$  in the arguments for the fermionic Green functions, and obtain

$$\begin{aligned} \iota \mathcal{S}_i^{m(4)} = & -\frac{|\eta_i|^4}{8} \int dt \sum_{\{k_i\}} \int \frac{d\omega}{2\pi} \\ & \times \text{Tr} \left[ \hat{g}_{k_{1\uparrow}}(\omega) \hat{A}_i(t) \hat{g}_{k_{2\downarrow}}(\omega) \hat{A}_i^*(t) \hat{g}_{k_{3\uparrow}}(\omega) \hat{A}_i(t) \hat{g}_{k_{4\downarrow}}(\omega) \hat{A}_i^*(t) \right]. \end{aligned}$$

For the retarded and advanced components, we have  $\sum_k = (\omega - \varepsilon_k / \hbar \pm i\delta)^{-1} \approx -i\pi\hbar\rho_0$ , where we assume that the real parts give zero. Then performing the  $\omega$ -integral, the fermions generate the following eight quartic terms in the effective magnon action

$$\begin{aligned} \iota \mathcal{S}_i^{m(4)} = & -\iota (\alpha_i^F)^2 \int dt \left[ u_{1i} a_i^{*c} a_i^{*c} a_i^c a_i^c - u_{1i} a_i^{*c} a_i^{*q} a_i^c a_i^c \right. \\ & + u_{2i} a_i^{*q} a_i^{*q} a_i^c a_i^c - u_{2i} a_i^{*c} a_i^{*q} a_i^q a_i^q + u_{3i} a_i^{*c} a_i^{*c} a_i^q a_i^q \\ & \left. + u_{3i} a_i^{*q} a_i^{*q} a_i^c a_i^c + u_{4i} a_i^{*c} a_i^{*q} a_i^c a_i^q + u_{5i} a_i^{*q} a_i^{*q} a_i^q a_i^q \right], \quad (\text{A1}) \end{aligned}$$

where

$$\begin{aligned} u_{1i} &= \pi \iota \frac{k_B T_F}{\hbar} \frac{\mu_s}{k_B T_F} \\ u_{2i} &= \pi \iota \frac{k_B T_F}{\hbar} \frac{5 \frac{\mu_s}{k_B T_F} + 3 \frac{\mu_s}{k_B T_F} \cosh\left(\frac{\mu_s}{k_B T_F}\right) - 8 \sinh\left(\frac{\mu_s}{k_B T_F}\right)}{\cosh\left(\frac{\mu_s}{k_B T_F}\right) - 1} \\ u_{3i} &= \pi \iota \frac{k_B T_F}{\hbar} \left[ 2 - \frac{\mu_s}{k_B T_F} \coth\left(\frac{\mu_s}{2k_B T_F}\right) \right] \\ u_{4i} &= -4\pi \iota \frac{k_B T_F}{\hbar} \left[ 1 - \frac{\mu_s}{k_B T_F} \coth\left(\frac{\mu_s}{2k_B T_F}\right) \right] \\ u_{5i} &= -\pi \iota \frac{k_B T_F}{\hbar} \coth\left(\frac{\mu_s}{2k_B T_F}\right) \text{csch}^2\left(\frac{\mu_s}{2k_B T_F}\right) \\ & \quad \times \left[ 3 \frac{\mu_s}{k_B T_F} + \frac{\mu_s}{k_B T_F} \cosh\left(\frac{\mu_s}{k_B T_F}\right) - 4 \sinh\left(\frac{\mu_s}{k_B T_F}\right) \right]. \end{aligned}$$

While the first 4 terms in Eq. (A1) renormalize the existing vertices in Eq. (4), the remaining terms are new quartic vertices are introduced by integration over the metallic bath.

\* Email: stakei@qc.cuny.edu

- <sup>1</sup> R. A. Duine, A. Brataas, S. A. Bender, and Y. Tserkovnyak, “Spintronics and Magnon Bose-Einstein Condensation,” in *Universal Themes of Bose-Einstein Condensation*, edited by N. P. Proukakis, D. W. Snoke, and P. B. Littlewood (Cambridge University Press, 2017) pp. 505–524.
- <sup>2</sup> C. Sun, T. Nattermann, and V. L. Pokrovsky, *J. Phys. D: Appl. Phys.* **50**, 143002 (2017).
- <sup>3</sup> H. Deng, H. Haug, and Y. Yamamoto, *Rev. Mod. Phys.* **82**, 1489 (2010).
- <sup>4</sup> M. H. Szymańska, J. Keeling, and P. B. Littlewood, “Non-equilibrium Bose-Einstein Condensation in a Dissipative Environment,” in *Quantum Gases*, Vol. 1 (Imperial College Press, 2011) pp. 447–459.
- <sup>5</sup> S. O. Demokritov, V. E. Demidov, O. Dzyapko, G. A. Melkov, A. A. Serga, B. Hillebrands, and A. N. Slavin, *Nature* **443**, 430 (2006).
- <sup>6</sup> V. E. Demidov, O. Dzyapko, S. O. Demokritov, G. A. Melkov, and A. N. Slavin, *Phys. Rev. Lett.* **99**, 037205 (2007).
- <sup>7</sup> V. E. Demidov, O. Dzyapko, S. O. Demokritov, G. A. Melkov, and A. N. Slavin, *Phys. Rev. Lett.* **100**, 047205 (2008).
- <sup>8</sup> A. A. Serga, V. S. Tiberkevich, C. W. Sandweg, V. I. Vasyuchka, D. A. Bozhko, A. V. Chumak, T. Neumann, B. Obry, G. A. Melkov, A. N. Slavin, and B. Hillebrands, *Nature Commun.* **5**,

3452 EP (2014).

- <sup>9</sup> V. E. Demidov, S. Urazhdin, B. Divinskiy, V. D. Bessonov, A. B. Rinkevich, V. V. Ustinov, and S. O. Demokritov, *Nature Commun.* **8**, 1579 (2017).
- <sup>10</sup> S. A. Bender, R. A. Duine, and Y. Tserkovnyak, *Phys. Rev. Lett.* **108**, 246601 (2012).
- <sup>11</sup> S. A. Bender, R. A. Duine, A. Brataas, and Y. Tserkovnyak, *Phys. Rev. B* **90**, 094409 (2014).
- <sup>12</sup> T. Wimmer, M. Althammer, L. Liensberger, N. Vlietstra, S. Geprägs, M. Weiler, R. Gross, and H. Huebl, arXiv:1812.01334 (2018).
- <sup>13</sup> J. Klaers, J. Schmitt, F. Vewinger, and M. Weitz, *Nature* **468**, 545 (2010).
- <sup>14</sup> J. P. Eisenstein and A. H. MacDonald, *Nature* **432**, 691 (2004).
- <sup>15</sup> J. Kasprzak, M. Richard, S. Kundermann, A. Baas, P. Jeambrun, J. M. J. Keeling, F. M. Marchetti, M. H. Szymańska, R. André, J. L. Staehli, V. Savona, P. B. Littlewood, B. Deveaud, and L. S. Dang, *Nature* **443**, 409 (2006).
- <sup>16</sup> M. H. Szymańska, J. Keeling, and P. B. Littlewood, *Phys. Rev. Lett.* **96**, 230602 (2006).
- <sup>17</sup> R. E. Troncoso, A. Brataas, and R. A. Duine, *Phys. Rev. B* **99**, 104426 (2019).
- <sup>18</sup> S. Sachdev, *Quantum Phase Transitions*, 2nd ed. (Cambridge University Press, Cambridge, 2011).

- <sup>19</sup> E. G. Batyev, Sov. Phys. JETP **62**, 173 (1985).
- <sup>20</sup> A. Kamenev, *Field Theory of Non-Equilibrium Systems* (Cambridge University Press, Cambridge, 2011).
- <sup>21</sup> Imaginary quartic coefficients for a dissipative Bose gas were obtained phenomenologically using a Markovian master equation approach in the context of exciton-polariton condensates.<sup>29</sup> The current work provides a concrete microscopic derivation for how these dissipative quartic vertices can arise in the context of a driven, dissipative magnon gas (see Appendix A for more details).
- <sup>22</sup> A. L. Fetter and J. D. Walecka, *Quantum Theory of Many-Particle Systems* (McGraw-Hill, Boston, 1971).
- <sup>23</sup> E. L. Fjærbu, N. Rohling, and A. Brataas, Phys. Rev. B **95**, 144408 (2017).
- <sup>24</sup> In the absence of the phonon bath, i.e.,  $\alpha_B = 0$ , we see from Eq. (18) that the instability occurs precisely when the nonequilibrium spin accumulation reaches the magnon gap (i.e.,  $\mu_s^c = \mu$ ). However, this threshold is raised in the presence of the phonons. This is reasonable because in the latter case, the drive must overcome additional decay to the phonons in order for the magnons to reach the critical density necessary for condensation. In Ref. 11,

the condition for instability toward magnon condensation was given by

$$\mu_s^c = \left(1 + \frac{\alpha_B}{2\alpha_F}\right)\mu,$$

which differs from Eq. (18) by a factor of 2 in front of  $\alpha_F$ . The factor arises in Ref. 11 because spin injection occurs at the metal-magnet boundary, which coincides with the antinodes of the thermal magnon normal modes. As evident from Sec. II, open boundaries are absent in the current work, so the factor of 2 does not arise here.

- <sup>25</sup> G. D. Mahan, *Many-Particle Physics*, 2nd ed. (Plenum Press, New York, 1990).
- <sup>26</sup> J. V. Alvarez and C. Gros, Phys. Rev. B **66**, 094403 (2002).
- <sup>27</sup> F. Meier, J. Levy, and D. Loss, Phys. Rev. Lett. **90**, 047901 (2003).
- <sup>28</sup> L. J. Cornelissen, J. Liu, B. J. van Wees, and R. A. Duine, Phys. Rev. Lett. **120**, 097702 (2018).
- <sup>29</sup> L. M. Sieberer, M. Buchhold, and S. Diehl, Rep. Prog. Phys. **79**, 096001 (2016).